2007-08-06

Texture memory and strain-texture mapping in a NiTi shape memory alloy

Ye, B.; Majumdar, B. S.; Dutta, I.

American Institute of Physics

Journal Name: Applied Physics Letters; Journal Volume: 91; Journal Issue: 6; Other Information: DOI: 10.1063/1.2768899; (c) 2007 American Institute of Physics; Country of input: International Atomic Energy Agency (IAEA)
https://hdl.handle.net/10945/60990

Texture memory and strain-texture mapping in a NiTi shape memory alloy

B. Ye and B. S. Majumdar[a)]
Materials Department, New Mexico Tech, 801 Leroy Place, Socorro, New Mexico 87801

I. Dutta
Center for Materials Science, Naval Postgraduate School, Monterey, California 93943

(Received 31 May 2007; accepted 15 July 2007; published online 9 August 2007)

The authors report on the near-reversible strain hysteresis during thermal cycling of a polycrystalline NiTi shape memory alloy at a constant stress that is below the yield strength of the martensite. *In situ* neutron diffraction experiments are used to demonstrate that the strain hysteresis occurs due to a *texture memory effect*, where the martensite develops a texture when it is cooled under load from the austenite phase and is thereafter "remembered." Further, the authors quantitatively relate the texture to the strain by developing a calculated strain-texture map or pole figure for the martensite phase, and indicate its applicability in other martensitic transformations.
 [DOI: 10.1063/1.2768899]

Shape memory alloys are known for their ability to recover from low-temperature permanent deformation of the martensite to the original shape when heated to above the austenite finish (A_f) temperature.[1,2] This recovery is aided by the low symmetry of the martensite phase ($B19'$ for NiTi), which assures that all the martensite variants following plastic deformation return to the original high symmetry austenite ($B2$) orientation on heating.[3] The martensitic transformation is nearly perfectly reversible under a combination of conditions, including stress, temperature, and magnetic field.[4–6] Most of the works[2,7] on NiTi alloys have focused either on plastic deformation of the martensite, or on stress-induced martensite formation during "superelastic" deformation slightly above the austenite start temperature A_s. The crystallographic theory of martensite[8] relies on a homogeneous lattice deformation that establishes lattice correspondence between variants of the martensite and parent austenite phase. The shear/shuffle[9] of atoms associated with the transformation requires low resistance to shear deformation, and this has been confirmed recently by experiments[10,11] as well as first-principles calculations,[12] which show that the shear modulus drops drastically in the neighborhood of the martensite start (M_s) temperature.

In this work, we focus on thermal cycling of a NiTi alloy at a low stress,[13,14] which is defined here as a stress below the plateau yield strength of the martensite below the martensite finish temperature M_f. Thus, this stress cannot cause any significant permanent strain of the martensite that can subsequently be recovered on heating above A_s. For a polycrystalline NiTi wire,[13] there was no measurable strain when it was thermally cycled at zero applied stress. However, strain hysteresis of up to 3% was observed when thermally cycled at a low stress. This phenomenon has not attracted much attention, and the only reported work on variant selection and associated strains during thermal cycling at constant stress is that on single crystals of NiTi uniaxially loaded along different crystal axes.[14] However, very little could be interpreted in terms of texture change, which is relevant to polycrystalline materials.

Here, we report on *in situ* neutron diffraction study during thermal cycling at constant stress to monitor the texture evolution of a rolled NiTi sheet sample. Neutron diffraction has been utilized to study the superelastic effect in bulk NiTi samples.[15,16] Associated texture changes may be obtained from changes in peak intensity, using general structure analysis system (GSAS) single peak fit and Rietveld refinement method.[17]

Hot rolled sheets of $Ni_{50.4}Ti_{49.6}$ atomic composition were purchased from Special Metals, Hartford, NY. Dogbone shaped tensile samples of $100\times5.7\times1.46$ mm^3 dimension were heat treated at 850 °C, followed by quenching in chilled water. All samples were dipped in liquid nitrogen to ensure pure $B19'$ phase prior to thermal cycling. The test samples were maintained at a constant tensile stress during thermal cycling between 25 and 90 °C, and macroscopic strain was monitored using an extensometer. Stress levels ranged between 20 and 150 MPa to confirm the generic nature of mechanical and texture response, and only the results at 150 MPa are reported here. In these *in situ* tests at the SMARTS (Ref. 18) facility at the Los Alamos National Laboratory (LANL), He detectors recorded diffraction patterns with diffraction vectors parallel and perpendicular to the load simultaneously. The heating/cooling rates were 4 °C/min, and neutron data were collected for 15 min at a given temperature following a 5 min equilibration. Following thermal cycling, texture maps were obtained at room temperature (RT) in the fully martensite state using the HIPPO (Ref. 19) instrument at LANL. Pole figures were calculated using GSAS Rietveld refinement and no symmetry was assumed.[17,18] Pole figures were plotted with generic mapping tools.[20] For inverse pole figures (IPFs) measured from SMARTS data, the same texture analysis procedures used by Von Dreele[21] were followed.

Figure 1 shows the strain-temperature curve during thermal cycling at a constant stress of 150 MPa, which is below the measured 0.2% offset yield strength of 235 MPa of the fully martensite material at RT. Very little change in strain occurred during initial heating. However, the very first cooling step was associated with large elongation, approximately 3.8% from C to E, even though the applied stress was well below the yield strength. Once this strain increase occurred, subsequent reheating simply acted to restore the original size

a)Electronic mail: majumdar@nmt.edu

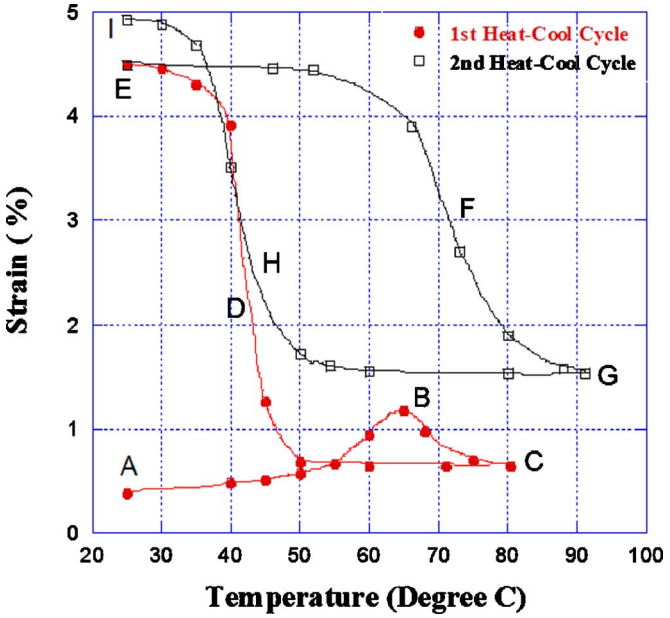

FIG. 1. (Color online) Macroscopic strain-temperature curve for a rolled NiTi sheet sample during thermomechanical cycling at 150 MPa applied stress. The strain path is indicated sequentially by the letters *A*, *B*, *C*, *D*, *E*, *F*, *G*, *H*, and *I*.

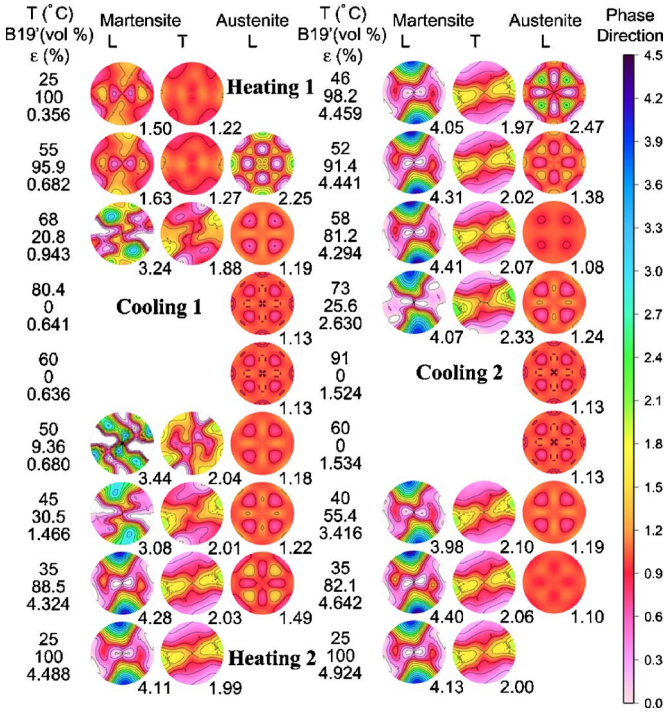

FIG. 2. (Color online) Inverse pole figures (IPFs), volume fraction (vol %), and macroscopic strain (ε,%) of martensite ($B19'$) and austenite ($B2$) in both the loading (L) and transverse (T) directions, during thermal cycling at 150 MPa applied stress. The maximum pole density in each IPF is marked at the right bottom corner. The center and rightmost point in the IPFs represent (001) and (100) poles, respectively, for the $B19'$ phase, while the top, right, and center directions are (001), (010), and (100) poles for the $B2$ phase, respectively.

of the austenite. Figure 1 shows that the austenite length was not fully recovered, however, this difference quickly decayed with subsequent cycles. Although the strain hysteresis appears similar to that known for the shape memory effect (SME), there are important differences. First, unlike traditional SME, a strain recovery on heating is observed even in the absence of low-temperature plastic deformation of the martensite. Second, the observed strain increase during the very first cooling step indicates that this response is not associated with a two-way shape memory behavior, where the latter requires many cycles of thermomechanical "training."[2,7]

Figure 2 shows the volume fraction of phases, the macroscopic strains, and the IPFs at different temperatures for both the $B2$ and $B19'$ phases. The color at each location or pole of the IPF quantifies the preference of that *hkl* pole (normal to the *hkl* plane) along defined laboratory directions. Specifically, these directions were the loading/longitudinal (L) or transverse (T) directions of the tensile sample. Leaving aside the first heating excursion for the time being, note that the texture of the martensite during the first cooling step is repeated during the second cooling step, and so on; compare, for example, the IPFs in the last row of Fig. 2. This repetition occurs even though the martensite phase disappears upon heating above ~80 °C, and reappears only after cooling below ~50 °C. Thus the martensite "remembers" its texture prior to heating to the austenite phase, and goes back to that state. We designate this phenomenon as a *texture memory* effect. In essence, the texture memory manifests as a reversible texture evolution during each cycle and this is believed to account for the macroscopic reversible strain phenomena. We also suspect that the sharp drop in modulus[10–12] that occurs at the transformation temperature allows the texture to develop even at a low applied stress.

We have used the shear/shuffle model to shed quantitative insight on the texture memory effect. Based on the 12 lattice correspondence variants known for the NiTi alloy,[14] and using the measured lattice parameters from our neutron diffraction measurements, $a_0=0.301\,79$ nm for the parent B2 phase and $a=0.289\,56$ nm, $b=0.464\,46$ nm, $c=0.412\,18$ nm, and $\gamma=97.41°$ for the monoclinic $B19'$ phase, the transformation strain can be calculated in the B2 crystal coordinate frame for each variant. Using the lattice correspondence variants relationship, the strain in a given direction can be calculated in both the $B2$ and $B19'$ coordinate frames. In a {001} stereographic projection for the $B19'$ phase, the transformation strain can be calculated for each pole direction, and further the strain distribution map can be constructed. One of the strain maps is shown in Fig. 3. One can show that the strain maps, calculated from the 12 correspondence variants expressed in the $B19'$ phase frame, are identical. In other words, the strain distribution map of Fig. 3 in the $B19'$ projection is *unique*.

An important feature of the calculated pole-strain map of Fig. 3 is that the region of negative strain occupies a far smaller area than the region of positive (tension) strain, and also the maximum strain magnitudes are different. This asymmetry has been observed before in the context of martensitic transformations in general. The maximum strain of about 11.7%, according to Fig. 3, occurs when the $(\bar{2}30)$ pole of different variants line up along the loading direction. In previous papers,[7,8] it has been suggested that those martensite variants that produce the largest longitudinal strain of the sample under simple tension would be selected. This would naturally favor a $(\bar{2}30)$ preferred pole along the loading axis. However, this orientation is not preferred in our experiments, likely because the transverse strains are not negative enough

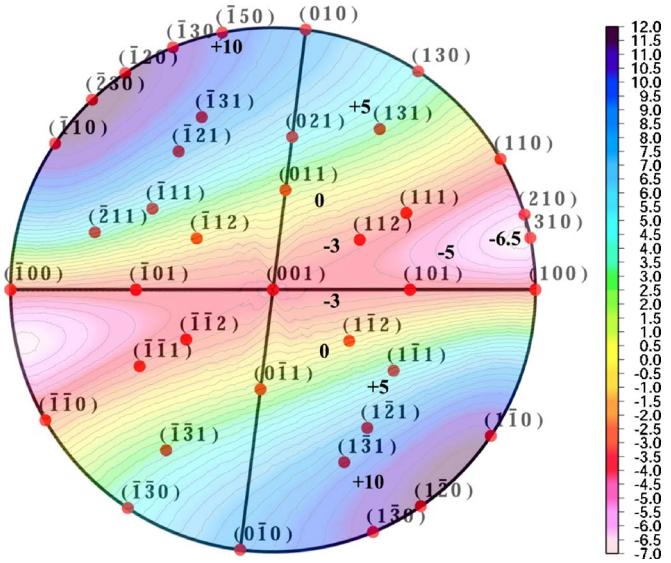

FIG. 3. (Color online) Calculated strain-texture map or pole figure in the martensite ($B19'$) phase corresponding to uniaxial loading. The poles are shown in brackets, and the contour lines represent values of strain in percent that results from transformation of $B2$ to the particular $B19'$ pole.

to result in a net volumetric strain close to zero for a uniaxial tension test. The transverse axis that produces the largest negative strain needs a near (310) pole alignment, with a $(\bar{1}50)$ pole that would then be along the specimen loading direction (see Fig. 3). Figure 2 shows that the martensite variants indeed have the highest $(\bar{1}50)$ pole density along the loading direction.

Figure 3 allows interpretation of the IPF of Fig. 2 and the mechanical data in Fig. 1. The austenite phase (points C and G) has negligible texture, and it gives rise to increasing volume fraction of martensite with a dominant $(\bar{1}50)$ texture along the loading direction as the sample is cooled under load. The martensite texture and volume fraction are then repeated in the next cycle and thereby the strain at any temperature. The primary exception is the first heating step, where the 850 °C treated sample was cooled *without* load. The increase from A to B occurs because the sample tries to take on the texture of a 150 MPa stressed sample. Since the martensite variants are heavily restricted (less glissile) until A_s is approached, the strain increase is initially negligible. However, the mobility of the remaining martensite is restored as A_s is crossed, so that the texture and strain (relative to austenite) at 68 °C (point B) in the first cycle does not differ significantly from those at 73 °C in the second heating cycle.

The HIPPO-generated pole figures (Fig. S1 on Ref. 22) at RT revealed that the as-received sample had low texture, although with slight preferred orientations of (011) and (100) poles along the loading direction. Following thermomechanical cycling, the preferred pole along the loading direction changed from (011) towards $(\bar{1}50)$, in excellent agreement with Figures 2 and 3. Tests at other stress levels produced similar mechanical response as Fig. 1, and the strain ranges were found to depend almost linearly on the stress (Fig. S2 on Ref. 22). Such stress-dependent strain response could be exploited in intelligent devices where different sizes or shapes may be obtained in the martensite state by simply controlling the stress during cooling. One additional important observation was that the dominant texture was dependent on the applied stress.

The strain-texture map in Fig. 3 can explain the peak intensity change observed by other researchers[15,16] during tension and compression tests of a superelastic NiTi alloy. For other martensite transformation processes, similar strain maps can be constructed. For example, we have obtained full agreement with IPFs that were observed by Field *et al.* for U–Nb alloys,[23] which were uniaxially deformed in tension and compression into the plateau regime of yielding. Generally, using the constructed strain map of the martensitic transformation process, the texture developed from loading process can be predicted semi-quantitatively, or conversely, it should be possible to obtain any desired texture by imposing the required external strain. Finally, it is possible that a similar behavior may occur in ferromagnetic materials, where, now, magnetic field (rather than temperature) and an imposed stress may be used to control size.

The authors thank Yang Liu of NMT for sample preparation, and D. W. Brown, B. Clausen, and S. Vogel of LANL for the neutron experiments. Funding from the NSF under NSF-DMR-0413852 and U.S. Army Research Office under ARO-42714MS are acknowledged. The work benefited from the Lujan Neutron Scattering Center, funded by the BES Office of DOE. LANL is operated under DOE Contract No. DE-AC52-06NA25396.

[1] W. J. Buehler, J. W. Gilfrich, and R. C. Wiley, J. Appl. Phys. **34**, 1475 (1963).
[2] K. Otsuka and X. Ren, Prog. Mater. Sci. **50**, 511 (2005).
[3] K. Bhattacharya and R. V. Kohn, Acta Mater. **44**, 529 (1996).
[4] R. Kainuma, Y. Imano, W. Ito, Y. Sutou, H. Morito, S. Okamoto, O. Kitakami, K. Oikawa, A. Fujita, T. Kanomata, and K. Ishida, Nature (London) **439**, 957 (2006).
[5] R. D. James and M. Wuttig, Philos. Mag. A **77**, 1273 (1998).
[6] R. C. O'Handley, J. Appl. Phys. **83**, 3263 (1998).
[7] C. M. Wayman, in *Physical Metallurgy*, edited by R. W. Cahn and P. Haasen (North-Holland Physics, New York, 1983), 2, Chap. 15, pp. 1032–1074.
[8] C. M. Wayman, *Introduction to the Crystallography of Martensitic Transformations* (Macmillan, New York, 1964).
[9] B. A. Hatt, J. Nucl. Mater. **19**, 133 (1966).
[10] X. Ren and K. Otsuka, Scr. Mater. **38**, 1669 (1998).
[11] T. M. Brill, S. Mittelbach, W. Assmus, M. Mullner, and B. Luthi, J. Phys.: Condens. Matter **3**, 9621 (1991).
[12] X. Y. Huang, G. J. Ackland, and K. M. Rabe, Nat. Mater. **2**, 307 (2003).
[13] Z. X. Wang, I. Dutta, and B. S. Majumdar, Scr. Mater. **54**, 627 (2006).
[14] H. Sehitoglu, R. Hamilton, D. Canadinc, X. Y. Zhang, K. Gall, I. Karaman, Y. Chumlyakov, and H. J. Maier, Metall. Mater. Trans. A **34A**, 5 (2003).
[15] R. Vaidyanathan, M. A. M. Bourke, and D. C. Dunand, J. Appl. Phys. **86**, 3020 (1999).
[16] P. Sittner, P. Lukas, V. Novak, M. R. Daymond, and G. M. Swallowe, Mater. Sci. Eng., A **378**, 97 (2004).
[17] A. C. Larson and R. B. Von Dreele, Los Alamos National Laboratory Report No. LAUR 86-748, 1994 (unpublished).
[18] M. A. M. Bourke, D. C. Dunand, and E. Ustundag, Appl. Phys. A: Mater. Sci. Process. **74**, 1707 (2002).
[19] H.-R. Wenk, L. Lutterotti, and S. Vogel, Nucl. Instrum. Methods Phys. Res. A **515**, 575 (2003).
[20] P. Wessel and W. H. F. Smith, EOS Trans. Am. Geophys. Union **76**, 329 (1995).
[21] R. B. Von Dreele, J. Appl. Crystallogr. **30**, 517 (1997).
[22] See EPAPS Document No. E-APPLAB-91-047732 for HIPPO and stress-strain plot. This document can be reached via a direct link in the online article's HTML reference section or via the EPAPS homepage (http://www.aip.org/pubservs/epaps.html).
[23] R. D. Field, D. W. Brown, and D. J. Thoma, Philos. Mag. **85**, 1441 (2005).